J. Fluid Mech. (1968), *vol.* 34, *part* 4, *pp.* 657–686
Printed in Great Britain

The stability of the laminar natural convection boundary layer

By C. P. KNOWLES† AND B. GEBHART
Sibley School of Mechanical Engineering, Cornell University, Ithaca, N.Y.

(Received 11 January 1968)

This paper concerns the stability characteristics of laminar natural convection in external flows. Until recently, very little was known about such stability because of the inherent complexity of temperature-coupled flows and because of the complicated mechanisms of disturbance propagation. In this work the stability of the laminar natural convection boundary layer is examined more closely in an attempt to predict the experimental results recently obtained. In particular, it is shown that an important thermal capacity coupling exists between the fluid and the wall which generates the flow. This thermal capacity coupling is shown to have a first-order effect for particular Grashof-number wave-number products. Solutions are obtained for a Prandtl number of 0·733 and several values of relative wall thermal capacity. These solutions indicate the important role of this wall coupling. In particular, the results predict the experimental data previously obtained.

In addition, solutions with 'zero wall storage' are obtained for a range of Prandtl numbers from 0·733 to 6·9. The relative disturbance u-velocity and temperature amplitudes and their phases are shown for $Pr = 0{\cdot}733$ and several wall-storage parameters, and for $Pr = 6{\cdot}9$ with zero wall storage. A comparison between the disturbance temperature distribution and the data obtained from a recent experimental investigation shows close agreement when the thermal capacity of the wall is taken into account.

In the appendix, it is shown that for temperature-coupled flows and wall-coupled boundary conditions the flow is unstable at a lower Grashof number for two-dimensional disturbances than it is for three-dimensional disturbances. This result has been supported by the recent experimental observations.

1. Introduction

The stability of the laminar fluid flows has been under investigation since the time of Lord Rayleigh. More recently, the laminar boundary layer stability has been analysed in an attempt to predict the transition from laminar to turbulent flow and also to gain a better understanding of the mechanism of turbulence.

The stability characteristics of the forced-flow Blasius boundary layer were successfully determined by the theoretical analyses of Tollmien (1931), Schlichting (1933) and Shen (1954). The agreement between the calculations and the

† Now at Systems, Science and Software, La Jolla, California

experimental data of Schubauer & Skramstad (1948) shows that, for this forced-flow case at least, the linearized small-disturbance theory is applicable for predicting the location and behaviour of the disturbances in the boundary layer around the neutral-stability point.

It is only comparatively recently that the stability of the natural convection boundary layer has received attention. This results perhaps from its increased complexity and also because the applications are more subtle. In the first analysis, by Plapp (1957), the comparable Orr–Sommerfeld type equations were formulated. These equations include the effect of temperature–velocity disturbance coupling, through the buoyancy term in the momentum equation. Estimates of conditions for neutral stability were made for a Prandtl number of 0·72 (air) for the isothermal-wall base-flow case. In obtaining these solutions, however, the temperature effect (coupling) was neglected.

The equations of Plapp (1957) were later rederived by Szewczyk (1962), who also used an asymptotic technique to obtain solutions for a Prandtl number of 10. The base flow was that of an isothermal wall and again the temperature coupling was neglected. Expansions were made about both the inner and outer critical layer. These calculations indicated that the flow is more unstable in the region of the outer critical layer. However, the stability limits predicted in both studies are significantly different from those based upon experimental data, including those obtained by Szewczyk, using water.

The first numerical solution of the stability characteristics of the natural convection boundary layer was obtained by Kurtz & Crandall (1962) for $Pr = 0{\cdot}733$. The base flow was that of an isothermal wall and again the effects of temperature coupling were neglected. The results of these calculations are significantly different from those of Plapp (1957).

The first solution which included temperature-coupling was obtained by Nachtsheim (1963). The velocity and temperature base flow profiles were those of an isothermal wall. The temperature-coupling between the momentum and energy disturbance equations was included; the complete set was solved. Solutions were obtained both with and without this temperature-coupling for Prandtl numbers of 0·733 (air) and 6·7 (water). A comparison between the coupled and uncoupled solutions at the same Prandtl number indicates that the effect of the temperature-coupling is very pronounced for lower values of the wave-number Grashof-number product. For the higher Prandtl number case, the inclusion of temperature-coupling shifts the predicted neutral-stability point to a lower value of the local Grashof number a minimum of a factor of 10^4. For the lower Prandtl number case, the shift is considerably smaller; however, for small wave-numbers (i.e. long wavelength disturbances) the coupling shifts the neutral curve to lower values of the minimum (or critical) Grashof number by as much as a factor of 50. These are tremendous differences in the prediction of the first point of laminar instability.

Prior to 1966 no experimental data were available to assess critically the applicability of the theory for natural convection flows nor to determine the importance of temperature-coupling. The experiments of Eckert & Soehngen (1951), Szewczyk (1962) and others were studies of the onset of naturally occurring

instability. In this type of instability the very small naturally occurring disturbances must be amplified by the boundary layer until they are large enough to be observed. As a result the 'neutral' Grashof number determined from such measurements depends strongly upon the magnitude of the ambient disturbances and also on the sensitivity of the instrument used to observe the boundary-layer fluctuations. Since the disturbances have undergone considerable amplification before they can be observed, it is impossible in this type of study to determine the location at which the flow is neutrally stable. The early attempts to introduce artificial disturbances in the boundary layer and observe their subsequent decay and reamplifications as they travel upstream had not been successful. Birch (1957) used a wire which was subjected to square-wave current pulses to introduce artificial disturbances. The frequency of the most unstable disturbances was correlated; however, Gartrell (1959), using the same apparatus, obtained different results.

A preliminary study, using artificially induced disturbances was undertaken by Colak-Antic (1964). The disturbances were introduced by means of an electrically pulsed wire. Because of a lack in the sensitivity of the measuring apparatus, no measurements were made in the region where the flow was neutrally stable.

The experimental study of Polymeropoulos (1966) provided the first carefully controlled experimental data. The stability of the uniform-flux boundary layer over a vertical flat plate in pressurized nitrogen was investigated. Controlled artificial disturbances were introduced by means of a vibrating ribbon, a technique used successfully by Schubauer & Skramstad (1948) in forced flow. The decay and amplification characteristics of disturbances as they travelled downstream were observed by means of an 8 in. Mach–Zehnder interferometer. By such techniques points of neutral stability could be clearly determined for various disturbance frequencies and wavelengths.

The results of this study (see Polymeropoulos & Gebhart 1967) are in general agreement with the coupled isothermal-wall results of Nachtsheim (1963). In particular, the data show the 'nose' at lower wave-numbers which was predicted by the temperature-coupled solution of Nachtsheim (1963).

In order to assess the difference in stability characteristics between uniform temperature and uniform-flux base flows, Polymeropoulos & Gebhart (1966) formulated the appropriate Orr–Sommerfeld type equations for the uniform-flux case. The uncoupled solution was obtained for a Prandtl number of 0·72. As in the isothermal-wall case, the uncoupled solution did not predict the 'nose' behaviour.

At the outset of this investigation, then, no information was available concerning the effect of temperature-coupling on the theoretical stability of other base flows such as, for example, the equally important uniform-flux boundary layer. This information is desirable both from a general point of view and also to provide a comparison for the experimental data of Polymeropoulos & Gebhart (1967). For the latter, it became apparent that it would be necessary to include the effects of the thermal storage characteristics of the heated wall used to generate the flow. This coupling between the fluid disturbance fluctuation and the

wall thermal capacity proved to have a pronounced first-order effect on the laminar stability predictions.

In addition, little information is available in the literature concerning the effect of Prandtl number on the laminar stability characteristics. An attempt at predicting the effect of Prandtl number was made by Sparrow, Tsou & Kurtz (1965), using the program developed by Kurtz & Crandall (1962). The minimum (or critical) Grashof number for neutral stability was calculated for several Prandtl-number cases. The effect of temperature coupling in the disturbance equations was neglected. The results of Nachtsheim (1963), which appeared previously, showed that this temperature-coupling is important, especially in predicting the critical Grashof number. In view of this, and also in preparation for an experimental study which will be reported later, the effect of Prandtl numbers from 0·733 to 6·9 was also investigated.

2. Theoretical analysis

Consider the laminar natural convection flow over a vertical flat plate with the co-ordinate system shown in figure 1. The base flow is assumed to be that resulting from a uniform surface heat flux at the inner boundary, neglecting viscous dissipation and compressibility effects (other than the buoyancy term in the momentum equation). For the stability analysis, the base flow is further assumed to be one-dimensional in that the derivatives of the base-flow quantities with respect to x are much smaller than those with respect to y. Hence, the base-flow quantities in the disturbance equations are considered to be functions of y only. The disturbance quantities are taken as small perturbations of the base-flow quantities. By a method similar to that of Squire (1933), it can be shown that the flow will be most unstable for two-dimensional disturbances (see appendix.) As a result, it is assumed that the disturbance quantities are functions of x, y and τ only. Using a development similar to that of Polymeropoulos & Gebhart (1966), it can be shown that for the uniform-flux case the disturbance equations can be written as

$$\frac{\partial \Omega}{\partial \tau} + U\frac{\partial \Omega}{\partial x} + v\frac{d^2U}{dy^2} = \nu\nabla^2\Omega + g\beta\frac{\partial t}{\partial y}, \tag{1}$$

where

$$\Omega = \frac{\partial u}{\partial y} - \frac{\partial v}{\partial x}$$

and

$$\frac{\partial t}{\partial \tau} + U\frac{\partial t}{\partial x} + v\frac{dT}{dy} = \frac{k}{\rho c}\nabla^2 t. \tag{2}$$

The continuity equation can be satisfied by introducing a disturbance stream function, ψ, such that $u = \partial\psi/\partial y$ and $v = -\partial\psi/\partial x$. Now any physical disturbance which is bounded can be represented by a Fourier series in which the wave-number (or frequency) of each term is an integer multiple of the zero-order term. It has been demonstrate experimentally by Polymeropoulos (1966), and can be concluded from the neutral curve, that for wavelengths which can be observed experimentally (i.e. wavelengths which are not too long), the first harmonic

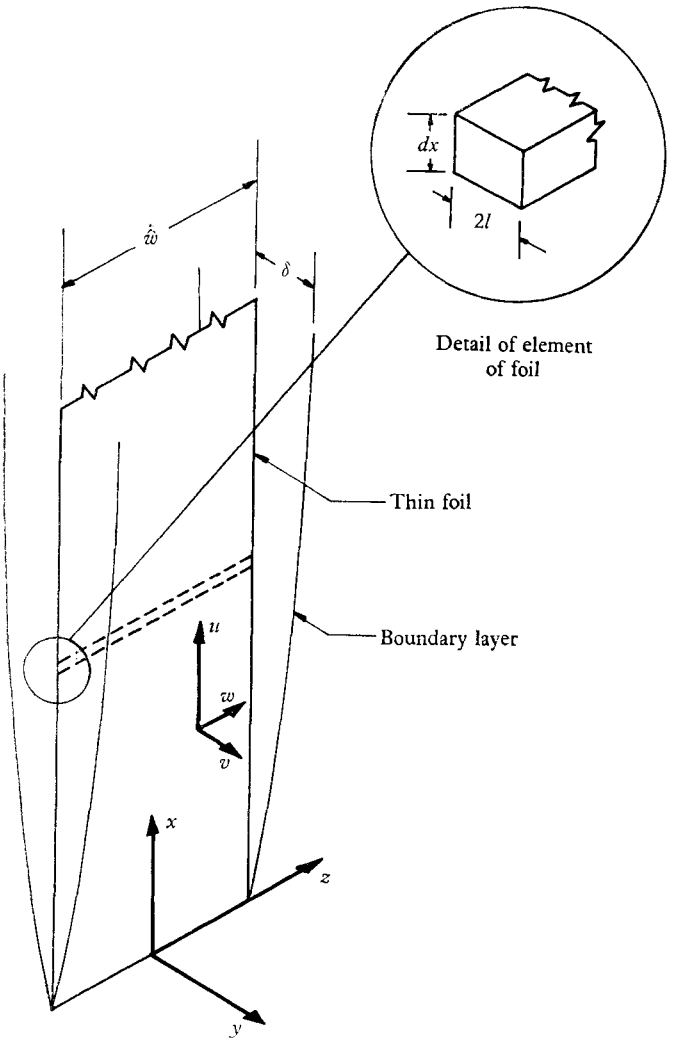

FIGURE 1. Co-ordinate system.

would be highly damped.† In view of this, it is sufficient to consider only one term in the series—that is, to examine whether a particular wavelength at a particular frequency is amplified or attenuated.‡ Thus the form of the disturbance can be defined as

$$\psi(x, y, \bar{\tau}) = \bar{\phi}(y) \exp[i(\bar{\alpha}x - \bar{\beta}\bar{\tau})],$$
$$t(x, y, \bar{\tau}) = \bar{s}(y) \exp[i(\bar{\alpha}x - \bar{\beta}\bar{\tau})], \tag{3}$$

where $\bar{\phi}$ and $\bar{s}$ are complex amplitude functions, $\mathrm{Re}(\bar{\alpha})$ is the wave-number in the x direction [$\mathrm{Re}(\bar{\alpha}) = 2\pi/\lambda$], and $\mathrm{Re}(\bar{\beta})$ is the frequency [$\mathrm{Re}(\bar{\beta}) = 2\pi f$]. The

† For very long wavelengths, the first harmonic may be in the amplified region of the neutral curve. Hence if this harmonic is present in the initial disturbance, it too will be amplified.

‡ This corresponds to obtaining solutions in terms of normal modes.

imaginary parts of $\bar{\alpha}$ and $\bar{\beta}$ give rise to amplification or attenuation of the disturbance wave. It is apparent that if $\mathrm{Im}\,(\bar{\alpha}) < 0$ the wave will amplify with increasing x, while if $\mathrm{Im}\,(\bar{\beta}) > 0$ the wave will amplify with increasing time. For the special case when $\mathrm{Im}\,(\bar{\alpha}) = \mathrm{Im}\,(\bar{\beta}) = 0$, the wave will be neutrally stable, neither amplifying nor decaying.

Equations (1) and (2) can be reduced to two ordinary differential equations by means of (3) and the following substitutions:

$$G^* = 5(Gr^*/5)^{\frac{1}{5}}, \quad \tau = \bar{\tau}U^*/\delta,$$
$$\delta = 5x/G^*, \quad \Phi = \bar{\phi}/U^*\delta,$$
$$\eta = y/\delta, \quad \alpha = \bar{\alpha}\delta,$$
$$U^* = \nu G^{*2}/5x, \quad \beta = \bar{\beta}\delta/U^*,$$
$$F' = U/U^*, \quad \xi = x/\delta,$$
$$H = \frac{T - T_\infty}{(q''x/k)}\left(\frac{Gr^*}{5}\right)^{\frac{1}{5}},$$
$$s = \frac{\bar{s}}{(q''x/k)}\left(\frac{Gr^*}{5}\right)^{\frac{1}{5}},$$

where

$$Gr^* = \frac{g\beta x^4 q''}{k\nu^2}$$

and q'' is the heat flux at the boundary, β is the coefficient of thermal volumetric expansion, g is the gravitational acceleration, k is the coefficient of thermal conductivity, ν is the kinematic viscosity and x is the distance from the leading edge. With the exception of the sign of H, these quantities are identical to those used by Polymeropoulos & Gebhart (1966). By using the negative of the conventional normalization for the temperature in the base flow, the resulting Orr–Sommerfeld equation will have the same form for the uniform flux and the isothermal-wall cases. This normalization will also give rise to base flow solutions for the two cases which can be more easily compared.

With the above substitutions, (1) and (2) can be reduced to

$$(F' - \beta/\alpha)(\Phi'' - \alpha^2\Phi) - F'''\Phi = \frac{-i}{\alpha G^*}(\Phi^{\mathrm{iv}} - 2\alpha^2\Phi'' + \alpha^4\Phi + s'), \tag{4}$$

$$(F' - \beta/\alpha)s - H'\phi = -\frac{i}{\alpha G^* Pr}(s'' - \alpha^2 s). \tag{5}$$

It should be noted that even though (4) and (5) are identical to the equations derived by Nachtsheim (1963) for the isothermal wall case, the base-flow velocity and temperature profiles will be different for the uniform-flux case. In addition, the surface-boundary conditions for the disturbances will, in general, be different for the two cases. As a result, the neutral curves for the two cases will also be different. It will also be shown subsequently that the disturbance-boundary conditions at the surface play a significant role in determining the shape of the neutral curve, and hence must be examined in some detail. This is the question of the coupling of the disturbances to the surface thermal capacity.

Equations (4) and (5) together constitute a sixth-order complex ordinary differential equation and six complex boundary conditions are required. The no-slip condition at the wall requires that

$$\text{at} \quad \eta = 0, \quad \Phi = \Phi' = 0.$$

In addition, in order to keep the disturbance energy finite, the disturbance velocities, disturbance temperature (and consequently the disturbance flux) must vanish as $\eta \to \infty$. Thus

$$\text{as} \quad \eta \to \infty, \quad \Phi \to 0, \quad \Phi' \to 0, \quad s \to 0.$$

The boundary conditions on the disturbance temperature and/or disturbance flux at the surface require further consideration. For the proper boundary condition at the wall, it is necessary to consider the thermal capacity of the heated element used to generate the flow. Clearly there are two limiting cases. If the wall is truly constant temperature (e.g. a wall with a very large thermal capacity and large thermal capacity and large thermal conductance normal to the surface) then flow disturbances will cause no surface-temperature disturbance. Therefore the proper disturbance-temperature boundary condition would be

$$\eta = 0, \quad s = 0 \quad \text{(high-thermal-capacity wall)}.$$

If, in addition, the wall has large thermal conductance parallel to the surface, the base flow will be that of an isothermal surface.

If, on the other hand, the wall has a truly constant energy input along its length (i.e. negligible internal conduction parallel to the surface) then the base flow will be that of a uniform flux wall. If the wall has, in addition, a zero thermal capacity, (e.g. a very thin electrically heated foil) the proper disturbance boundary condition is zero disturbance in the surface heat flux. That is

$$\text{at} \quad \eta = 0, \quad s' = 0 \quad \text{(zero thermal capacity wall)}.$$

It was found that the limiting cases $s = 0$ and $s' = 0$ were not sufficient to explain, e.g. the experimental results of Polymeropoulos & Gebhart (1967). Based on the results of Gebhart (1963) for transient natural convection and on the implications of Dunn & Lin (1955) for forced-flow stability, it was expected that the physical properties of the electrically heated foil used to generate the base flow in the study of Polymeropuolos & Gebhart (1967) and in any similar study would require a more realistic surface boundary condition for the disturbance temperature and the disturbance flux. This is now known to be necessary even though it had been experimentally verified that the base-flow wall temperature distribution for thin electrically heated foils corresponds closely to that predicted by theory for a uniform flux wall. There is inevitably a non-negligible thermal capacity effect.

In order to establish the proper boundary conditions, consider an element of a thin foil such as that used in the experimental study. For a thin foil the conduction in the vertical direction can be neglected.

An energy balance on an element (shown in figure 1) is written

$$I^2\left(\frac{\rho_e dx}{\hat{w}\hat{l}}\right) = (\rho \hat{w} \hat{l} \hat{c})_{\text{foil}} dx \left(\frac{dt}{d\bar{\tau}}\right)_0 - (k\hat{w})\, dx \left(\frac{dT}{dy}\right)_0 - (k\hat{w})\, dx \left(\frac{dt}{dy}\right)_0, \tag{6}$$

where ρ_e is the electrical resistivity of the foil, I is the foil current, T is the base-flow temperature and t is the disturbance temperature. The zero subscript indicates that the derivatives are evaluated at $y = 0$. Subtracting the steady base flow quantities from (6) yields the relation

$$(\rho l\hat{c})_{\text{foil}} \left(\frac{dt}{d\bar{\tau}}\right)_0 - k\left(\frac{dt}{dy}\right)_0 = 0. \tag{7}$$

Equation (7) can be normalized in the same way as (4) and (5). The result is the appropriate disturbance temperature boundary condition,

$$s(0) = \left(\frac{i}{Q^* G^{*2} \beta}\right) s'(0), \tag{8}$$

where

$$Q^* = \frac{1}{5} \frac{(\rho l\hat{c})_{\text{foil}}}{x_n (k/\nu)_{\text{fluid}}} = \left(\frac{Pr}{5}\right) \frac{(\rho l\hat{c})_{\text{foil}}}{(\rho x_n \hat{c})_{\text{fluid}}} \tag{9}$$

and x_n is the vertical location of the neutral stability point. (x_n can be determined from the value of G^* for neutral stability.) The Q^*, defined by (9), is a thermal capacity term similar to that defined by Gebhart (1963) for the transient convection case.†

Equation (8) contains the two extreme disturbance boundary conditions, since $s(0)$ and $s'(0)$ are bounded. A foil with zero thermal capacity corresponds to $Q^* = 0$. Hence (8) requires that $s'(0) = 0$, which is the pure uniform flux boundary condition. If, on the other hand, the foil has a very large thermal capacity compared to that of the fluid, then $Q^* \to \infty$ and (8) reduces to the condition that $s(0) = 0$, corresponding to the isothermal-wall disturbance temperature-boundary condition. It should be noted that even for the latter case, the base flow may still conform to the uniform flux solution, as in the study by Polymeropoulos & Gebhart (1967), because of negligible streamwise conduction in the foil.

3. Method of solution

Equations (4) and (5) were numerically integrated on a Control Data 1604 computer using a technique similar to that of Nachtsheim (1963). These equations constitute a two-point boundary-value problem with two unknown eigenvalues. The disturbance boundary conditions at infinity were transformed into equivalent boundary conditions at the edge of the base-flow boundary layer since the analytical solution to the disturbance equations could be obtained in this outer region (see Nachtsheim 1963). This outer solution was matched to the inner solution to provide the complete solution.

In order to start the step-by-step integration to obtain the inner solution, three complex boundary conditions must be guessed in addition to the eigenvalues, in order to begin the integration. Since the equations are linear and homogeneous, one of these boundary conditions can be specified arbitrarily

† Typical values of Q^* for various fluids are shown in the table. The effect of this boundary condition on stability will be shown in the results which follow.

(except that it must be finite and non-zero). This choice will simply fix the size of the solution. For this purpose, it is convenient to specify that $\Phi''(0) = 1$. Guesses are then made for the values of $\Phi'''(0)$ and $s(0)$ [or $s'(0)$, depending upon the magnitude of Q^*]. It is also necessary to guess one eigenvalue pair. In the solutions obtained by Nachtsheim (1963) and Polymeropoulos & Gebhart (1966), the real and imaginary parts of the complex wave velocity, c (where $c = \beta/\alpha$), were chosen as eigenvalues to be determined for particular preset values of α and G^*. The solution obtained for a given α, G^* set would yield a non-zero value of the imaginary part of c indicating that the disturbance would either amplify or decay with time. This procedure required the complete set of equations to be solved several times with different values of G^* until the imaginary part of c changed sign. Then Im (c) could be plotted as a function of G^* and the value of G^* determined which would yield Im $(c) = 0$.

At best this technique requires at least two complete solutions and in general at least three of four. An additional solution is required for the proper G^* to determine the eigenfunctions at the neutral stability point.

In order to eliminate this difficulty, Im (α) and Im (β) were both set equal to zero identically. The eigenvalues are then Re (α) and Re (β). Thus for a given Prandtl number and G^* parameter, a solution was obtained for

$$\text{Im}\,(\alpha) = \text{Im}\,(\beta) = 0.$$

Each solution which was obtained by this method represented a solution of the neutral stability equations.

The integration was accomplished by a sixth-order Adams integration scheme which used a Runge–Kutta integration to generate the required back points. A step size of $\Delta\eta = 0{\cdot}1$ was used. The effect of step size was checked by recomputing some of the results with $\Delta\eta = 0{\cdot}05$. The new eigenfunctions and eigenvalues agreed with the old values to better than $0{\cdot}05\,\%$. As a result the step size of $\Delta\eta = 0{\cdot}1$ was used in all calculations.

Each new solution was obtained by using the starting values from the previous solution and incrementing the value of G^* by an amount of ΔG^*. If a satisfactory solution was not obtained within a preset number of iterations (usually 10–20) then the value of ΔG^* was halved and the procedure was repeated. Typical values of ΔG^* are 5 in the range of $G^* < 120$. As G^* became larger the allowable values of ΔG^* were reduced.

For lower values of $\alpha G^* Pr$ and αG^*, single precision arithmetic was satisfactory for convergence. For higher values of these parameters, however, double precision was used to obtain proper convergence, in order to obtain the correct eigenfunctions. A Newton–Raphson scheme was used to correct the guesses of the starting values and the eigenvalues. The derivatives for this scheme were obtained by differentiating (4) and (5) with respect to the starting values and eigenvalues, a technique which was also used by Nachtsheim (1963).

The equations for the derivatives with respect to $\Phi'''(0)$ and $s(0)$ or $s'(0)$ are identical to those derived by Nachtsheim (1963). The boundary conditions for the later equations will be different, however, because of the inclusion of the thermal capacity of the plate. If Q^* is small, then $s'(0)$ is also small. For this

circumstance, it is appropriate to guess the value of $s(0)$ and determine $s'(0)$ from (8). If $s(0) = \sigma$ then the appropriate boundary conditions for the derivative equations with respect to σ are

$$\Phi_\sigma(0) = \Phi'_\sigma(0) = \Phi''_\sigma(0) = \Phi'''_\sigma(0) = 0,$$
$$s_\sigma(0) = 1,$$
$$s'_\sigma(0) = -iQ^*G^{*2}\beta.$$

If, on the other hand, Q^* is large, then $s(0)$ is small. In this case, the value of $s'(0)$ is guessed to be σ, and the value of $s(0)$ is obtained from (8). For this case the boundary conditions for the derivative equations are

$$\Phi_\sigma(0) = \Phi'_\sigma(0) = \Phi''_\sigma(0) = \Phi'''_\sigma(0) = 0,$$
$$s'_\sigma(0) = 1$$

and

$$s_\sigma(0) = i/Q^*G^{*2}\beta.$$

Because of a different choice of eigenvalues, the derivatives of (4) and (5) with respect to the eigenvalues will be different from those of Nachtsheim. These equations, which must also be integrated are

$$\left.\begin{aligned}(F'-\beta/\alpha)(\Phi''_\alpha-\alpha^2\Phi_\alpha-2\alpha\Phi)+\frac{\beta}{\alpha^2}(\Phi''-\alpha^2\Phi)-F'''\Phi_\alpha \\ =-\frac{i}{\alpha G^*}(\Phi^{\mathrm{iv}}_\alpha-2\alpha^2\Phi''_\alpha+\alpha^4\Phi_\alpha+s'_\alpha-4\alpha\Phi''+4\alpha^3\Phi) \\ +\frac{i}{\alpha^2G^*}(\Phi^{\mathrm{iv}}-2\alpha^2\Phi''+\alpha^4\Phi+s')\end{aligned}\right\} \tag{10}$$

and

$$(F'-\beta/\alpha)s_\alpha+\frac{\beta}{\alpha^2}s-H'\Phi_\alpha=-\frac{i}{\alpha G^*Pr}(s''_\alpha-\alpha^2S_\alpha-2\alpha s)+\frac{i}{\alpha^2G^*Pr}(s''-\alpha^2s), \tag{11}$$

with the boundary conditions

$$\Phi_\alpha(0) = \Phi'_\alpha(0) = \Phi''_\alpha(0) = \Phi'''_\alpha(0) = s_\alpha(0) = s'_\alpha(0) = 0$$

and

$$(F'-\beta/\alpha)(\Phi''_\beta-\alpha^2\Phi_\beta)-\frac{1}{\alpha}(\Phi''-\alpha^2\Phi)-F'''\Phi_\beta=-\frac{i}{\alpha G^*}(\Phi^{\mathrm{iv}}_\beta-2\alpha^2\Phi''_\beta+\alpha^4\Phi_\beta+s'_\beta) \tag{12}$$

and

$$(F'-\beta/\alpha)s_\beta-H'\Phi_\beta-\frac{s}{\alpha}=-\frac{i}{\alpha G^*Pr}(s''_\beta-\alpha^2s_\beta) \tag{13}$$

with the boundary conditions

$$\Phi_\beta(0) = \Phi'_\beta(0) = \Phi''_\beta(0) = \Phi'''_\beta(0) = 0$$

and

$$\beta s_\beta(0)+s(0) = \frac{i}{Q^*G^{*2}}s'_\beta(0).$$

As in the method of Nachtsheim, these derivative equations must be integrated along with the main disturbance equations. It is apparent that by specifying both Im (α) and Im (β) to be zero, it is necessary to integrate an additional set of

six first-order complex equations, making a total of 60 real first-order equations which must be integrated. If the eigenvalues were taken as Re (c) and Im (c), as in the case of Nachtsheim (1963), the Cauchy-Reimann equations could be used to reduce this number to 48. Since this set would have to be integrated several times in order to obtain a neutral solution however, it is expedient to use the present method.

4. Results

The results which were obtained from the numerical integration were curves of neutral stability for the uniform flux base flow, including temperature coupling, for various values of Q^* (relative thermal capacity of the wall) and Prandtl number. A curve divides the (α, G^*) or (β, G^*) plane into regions in which a particular disturbance (characterized by the α, G* co-ordinates) will be either stable or unstable.

The results for a Prandtl number of 0·733 (corresponding to air) are shown in figures 2 and 3. The widely diverse character of the neutral curves for various values of Q^* is readily apparent. For reference, the uncoupled solution of Polymeropoulos & Gebhart (1966) for the uniform flux base flow is also shown.

These results predict that the thermal capacity of the wall will have a pronounced effect on the stability of the flow. For finite but non-zero values of Q^*, the boundary condition depends upon the values of G^* and β. From (8) it can be seen that as $G^* \to 0$, the boundary condition becomes asymptotic to $s'(0) = 0$. Hence it is only for the intermediate values of G^* that the more precise boundary condition departs from the limiting cases.

In addition, the effect of Prandtl number on the limiting case of a purely uniform flux wall of zero relative thermal capacity [i.e. $Q^* = 0$ and $s'(0) = 0$] was investigated. The results of these calculations, shown in figures 4 and 5, show entirely different limiting behaviour (for $s'(0) = 0$) as α (and β) $\to 0$.

The eigenfunction information obtained from the integrations for $Pr = 0{\cdot}733$ and various values of Q^* and for higher Prandtl number with $Q^* = 0$ show many interesting characteristics and trends. Some of this information is sharply at variance with the point of view and method of analysis used in many early estimates of approximate solutions of the Orr–Sommerfeld equations. Certain aspects of the results are discussed below in the terms of the calculated velocity and temperature disturbance distributions.

The relative neutral disturbance velocity and temperature distributions can be obtained from the eigenfunctions as follows:

$$\frac{u}{U^*} = [(\Phi'_{\mathrm{Re}})^2 + \Phi'^2_{\mathrm{Im}}]^{\frac{1}{2}} \cos[\alpha\xi - \beta\tau + \Theta_u], \tag{14}$$

$$\frac{v}{U^*} = \alpha[(\Phi_{\mathrm{Re}})^2 + (\Phi_{\mathrm{Im}})^2]^{\frac{1}{2}} \sin[\alpha\xi - \beta\tau + \Theta_v] \tag{15}$$

and

$$\frac{t}{q''x/k}\left(\frac{Gr^*}{5}\right)^{\frac{1}{5}} = [(s_{\mathrm{Re}})^2 + (s_{\mathrm{Im}})^2]^{\frac{1}{2}} \cos[\alpha\xi - \beta\tau + \Theta_t], \tag{16}$$

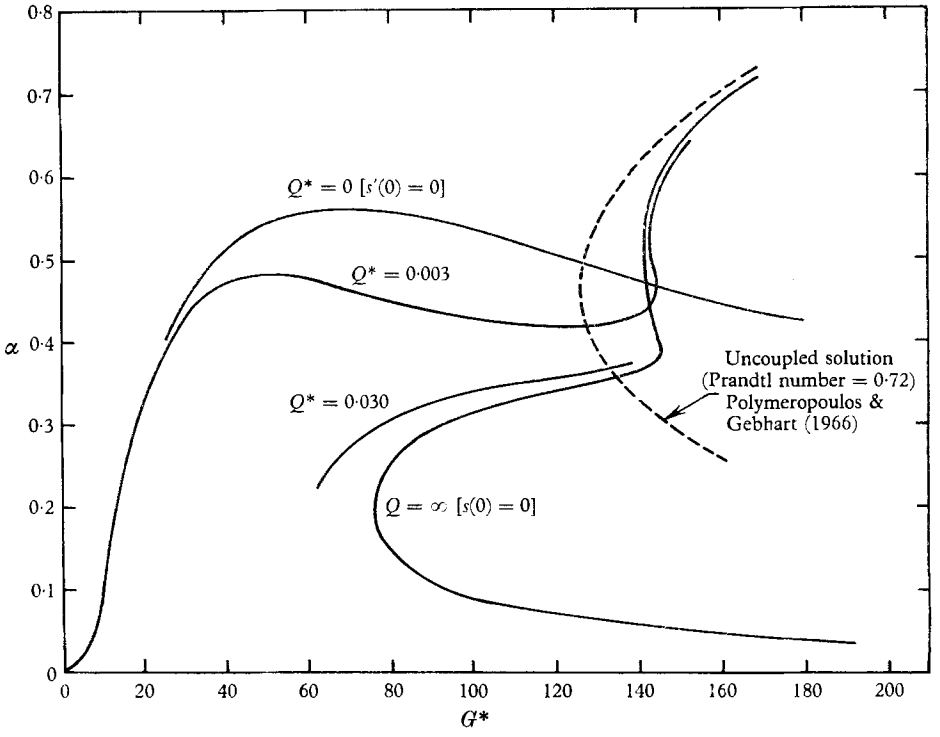

FIGURE 2. Wave-number neutral curve for uniform flux base flow and Prandtl number = 0·733.

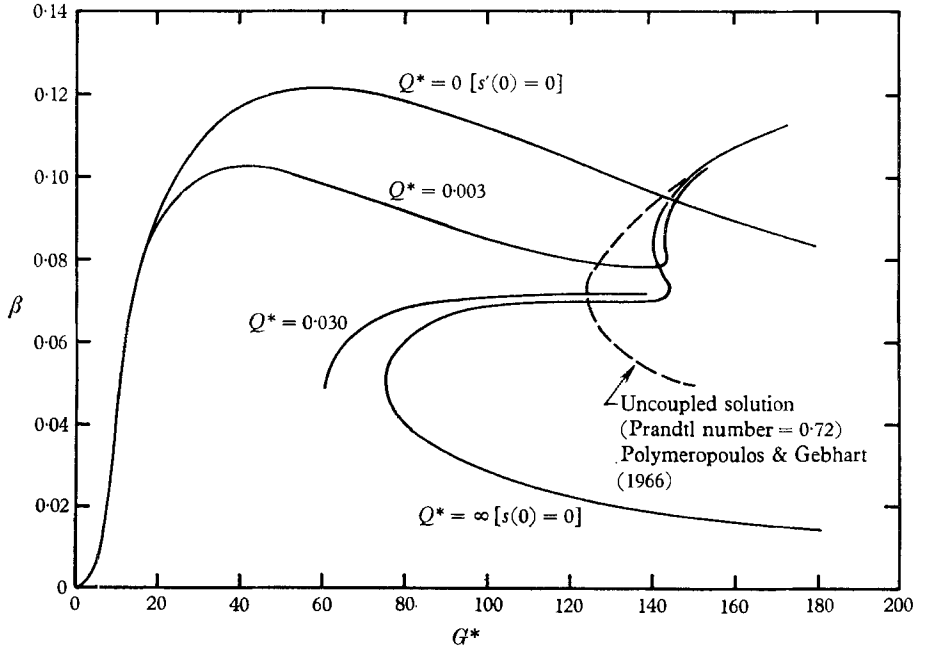

FIGURE 3. Frequency neutral curve for uniform flux base flow and Prandtl number = 0·733.

where the phase angles Θ_u, Θ_v and Θ_t are defined by

$$\Theta_u = \tan^{-1}(\Phi'_{\mathrm{Im}}/\Phi'_{\mathrm{Re}}), \tag{17}$$

$$\Theta_v = \tan^{-1}(\Phi_{\mathrm{Im}}/\Phi_{\mathrm{Re}}) \tag{18}$$

and

$$\Theta_t = \tan^{-1}(s_{\mathrm{Im}}/s_{\mathrm{Re}}). \tag{19}$$

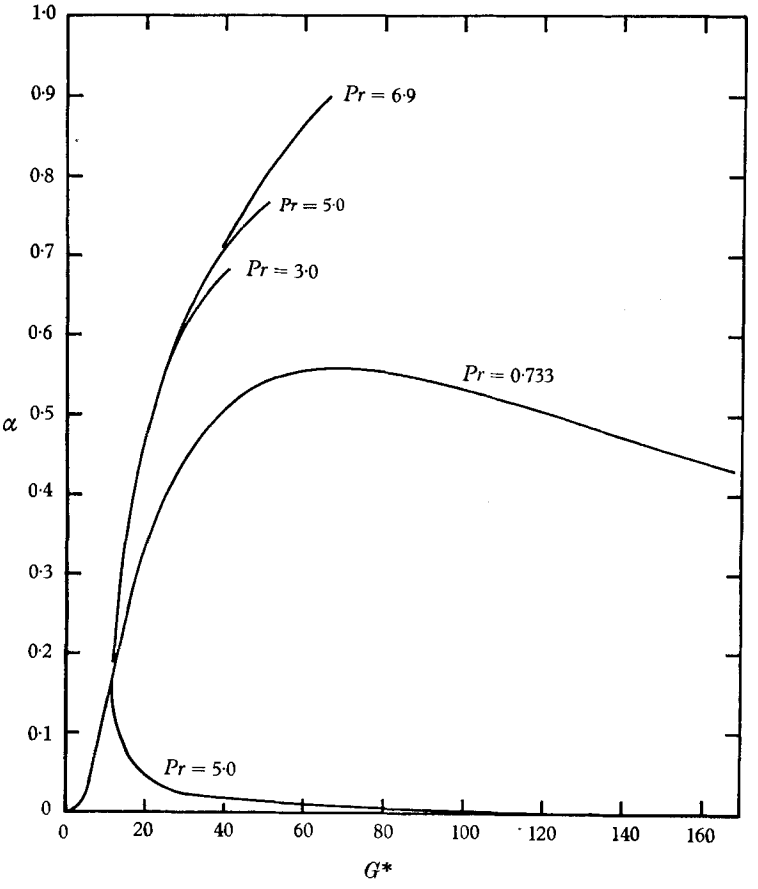

FIGURE 4. Effect of Prandtl number on the wave-number neutral curve for uniform flux base flow and $s'(0) = 0$ ($Q^* = 0$).

Since the disturbance equations are linear and homogeneous, the absolute magnitude of the disturbances cannot be obtained. As a result, these disturbance amplitude equations are normalized by their maximum values so that

$$\frac{u}{u_{\max}} = \left[\frac{(\Phi'_{\mathrm{Re}})^2 + (\Phi'_{\mathrm{Im}})^2}{[(\Phi'_{\mathrm{Re}})^2 + (\Phi'_{\mathrm{Im}})^2]_{\max}}\right]^{\frac{1}{2}}, \tag{20}$$

$$\frac{v}{v_{\max}} = \left[\frac{(\Phi_{\mathrm{Re}})^2 + (\Phi_{\mathrm{Im}})^2}{[(\Phi_{\mathrm{Re}})^2 + (\Phi_{\mathrm{Im}})^2]_{\max}}\right]^{\frac{1}{2}}, \tag{21}$$

$$\frac{t}{t_{\max}} = \left[\frac{(s_{\mathrm{Re}})^2 + (s_{\mathrm{Im}})^2}{[(s_{\mathrm{Re}})^2 + (s_{\mathrm{Im}})^2]_{\max}}\right]^{\frac{1}{2}}. \tag{22}$$

The neutrally stable relative disturbance u-velocity and disturbance temperature distributions across the boundary region are plotted in figures 6 to 10 for

various values of Pr, Q^*, α and G^*. These results show clearly the effect of the temperature boundary condition. For a truly uniform flux wall ($Q^* = 0$) the temperature disturbance remains large near the wall, as shown in figures 6 and 7. Figures 7 to 10 indicate that the disturbance temperature distribution is only a weak function of the G^* parameter for a Prandtl number of 0·733, although it is a strong function of the Prandtl number, as shown by figures 6 and 7.

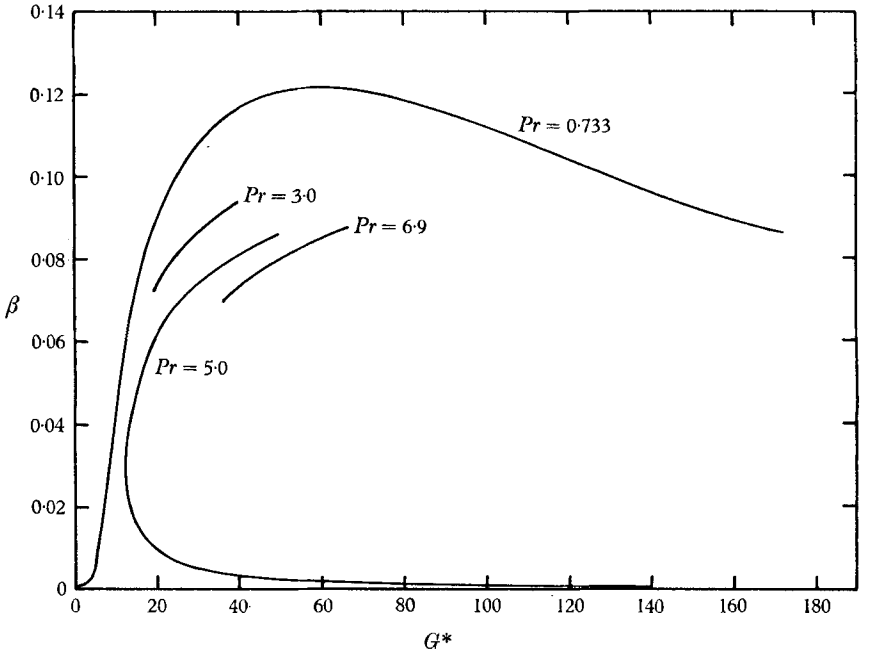

FIGURE 5. Effect of Prandtl number on the frequency neutral curve for uniform flux base flow and $s'(0) = 0$ ($Q^* = 0$).

The disturbance u-velocity distributions depend strongly upon both the Prandtl number and Grashof parameter, G^*. The distributions for the lower values of G^* show a single inner peak and another peak occurring at the edge and just outside the thermal boundary layer for $Pr = 0{\cdot}733$ and $Pr = 6{\cdot}9$, respectively. For higher values of G^*, for $Pr = 0{\cdot}733$, a third local maximum occurs in the disturbance velocity distribution. For $Pr = 0{\cdot}733$ the maximum disturbance velocity occurs at the approximate location of either the outer critical layer or the inflexion point of the base flow (except for the case of $G^* = 167$ with $s(0) = 0$, figure 10). The maximum in the velocity distribution occurs at about the same location as the disturbance temperature maximum (except for the case noted). For the solutions with $Q^* = 0$ (corresponding to $s'(0) = 0$) it can be seen that the u-velocity maximum occurs near the outer critical layer. As Q^* increases, this behaviour changes. For $Q^* = \infty$ (corresponding to $s(0) = 0$) and $Pr = 0{\cdot}733$, it can be seen from figure 10 that the disturbance velocity maximum becomes fixed approximately at the inflexion point, regardless of the location of the outer critical layer.

The influence of the inner critical layer can also be observed in these figures. A second local maximum occurs in the vicinity of the inner critical layer. The magnitude of this local maximum depends upon the value of G^*. For G^* sufficiently large, figure 10 shows that this maximum can actually exceed the value of the outer critical layer (or inflexion point). The fact that the location does not correspond exactly to the inner critical layer is presumably due to the temperature coupling.

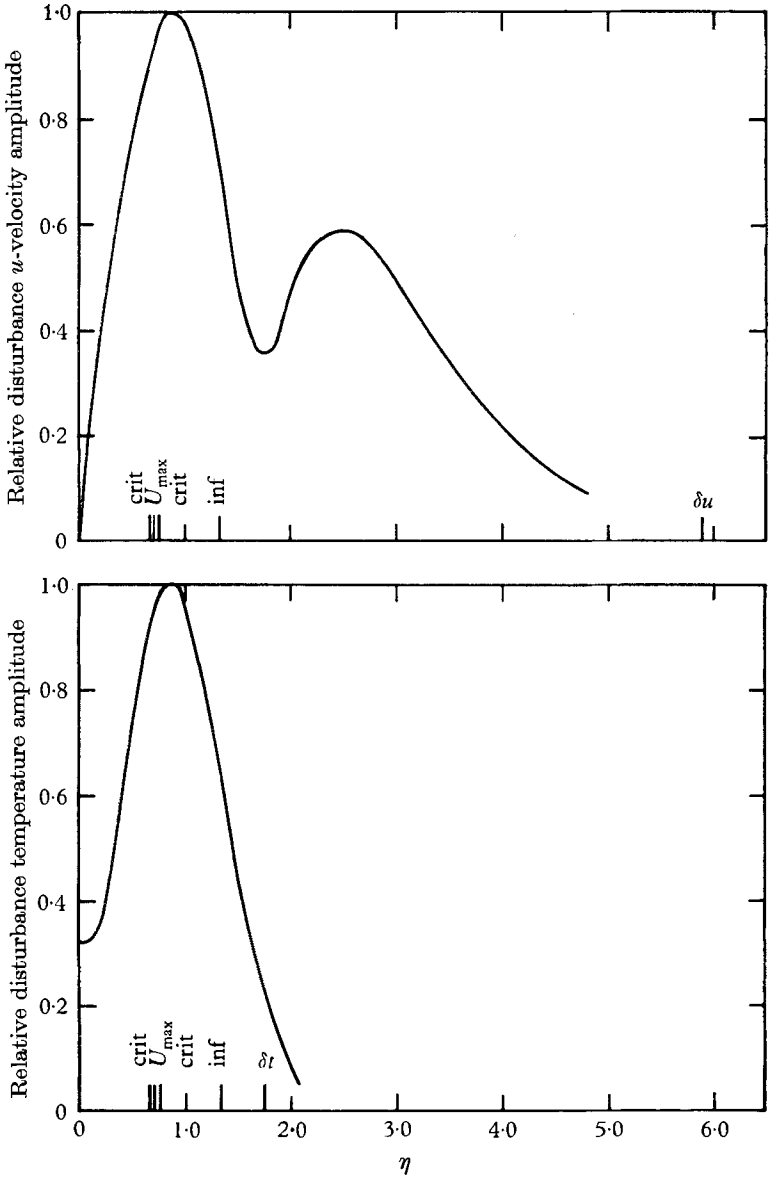

FIGURE 6. Theoretical disturbance amplitude distributions for Prandtl number = 6·9, uniform flux base flow and $s'(0) = 0$ ($Q^* = 0$). δu and δt indicate the outer edges of the velocity and thermal boundary layers.

For $Pr = 0{\cdot}733$ and for the extreme of $Q^* = 0$, the disturbance temperature distribution has a maximum which occurs inside the outer critical layer. For small values of Q^*, however, the location shifts toward the inflexion point location. This shift is apparent even for $Q^* = 0{\cdot}003$. For $Q^* = \infty$, the locations are essentially coincident.

The various disturbance temperature distributions show very clearly the im-

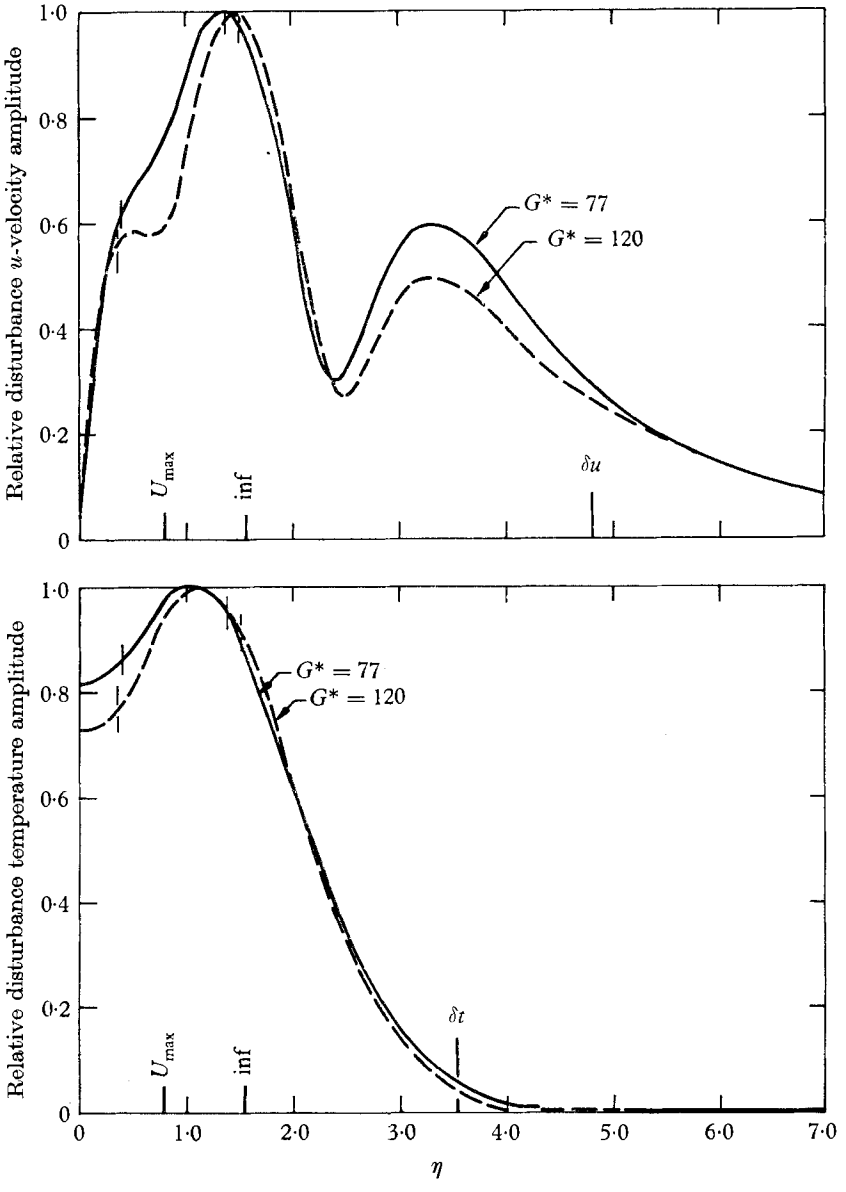

FIGURE 7. Theoretical disturbance amplitude distributions for Prandtl number = 0·733, uniform flux base flow and $s'(0) = 0$ ($Q^* = 0$). Vertical lines indicate the locations of the critical layers. δu and δt indicate the outer edges of the velocity and thermal boundary layers.

portance of the thermal boundary condition on the solutions of the stability equations. For a wall with low thermal capacity, the disturbance temperature at the wall in air can have an amplitude of up to 80 % of its maximum value, in the base flow corresponding to that of a uniform flux wall. In many applications this would amount to a very important surface temperature disturbance effect.

The phase angle of these disturbance quantities was computed from (17) to (19). The results are shown in figures 11 and 12 for a Prandtl number of 0·733 and

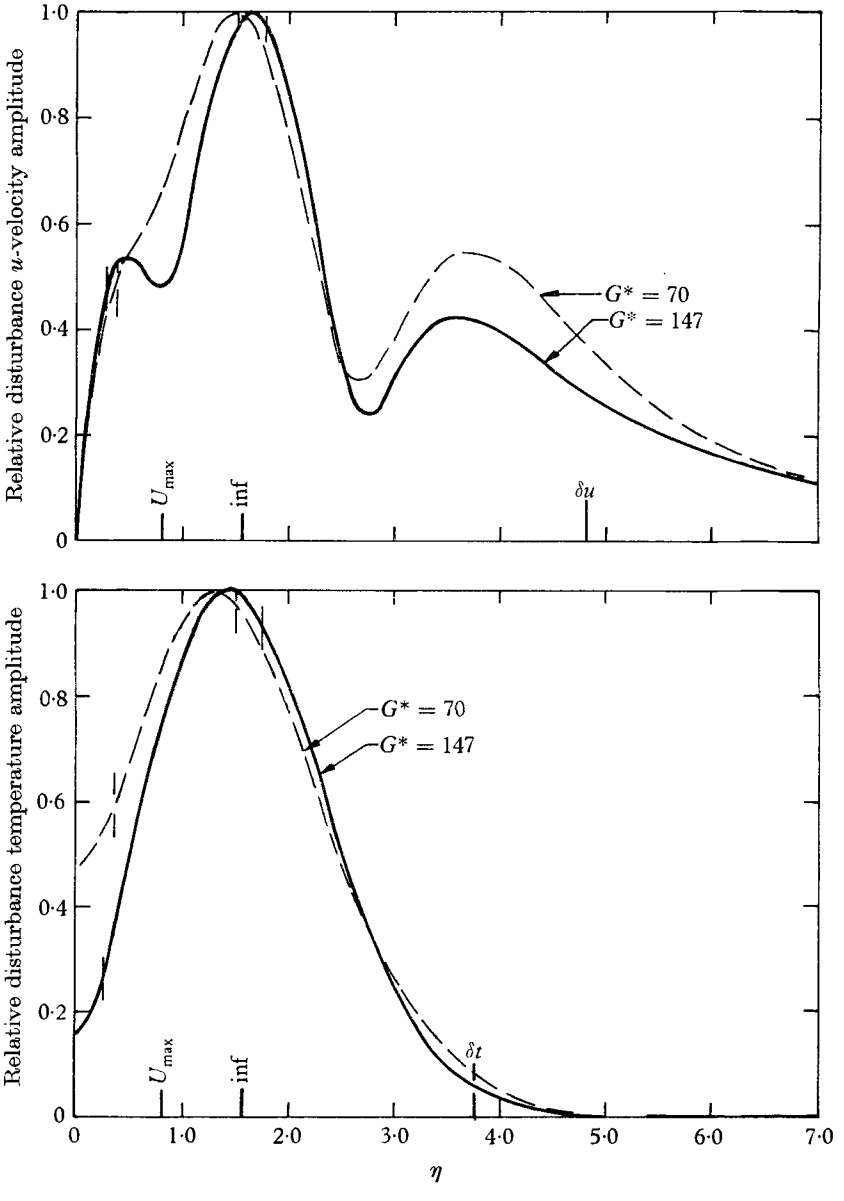

FIGURE 8. Theoretical disturbance amplitude distributions for Prandtl number = 0·733, uniform flux base flow and $Q^* = 0{\cdot}003$. Vertical lines indicate the locations of the critical layers. δu and δt indicate the outer edges of the velocity and thermal boundary layers.

figure 13 for a Prandtl number of 6·9. For the air case, it can be seen that the disturbance temperature phase distribution depends slightly upon the temperature boundary condition. For both boundary conditions, i.e. for large and zero relative thermal capacity, and for a range of G^*, the disturbance temperature undergoes a gradual phase change of approximately $\frac{1}{4}$-wave across the thermal boundary layer for $Pr = 0{\cdot}733$. The phase distribution for the disturbance temperature with a Prandtl number of 6·9 and $s'(0) = 0$ shows a similar be-

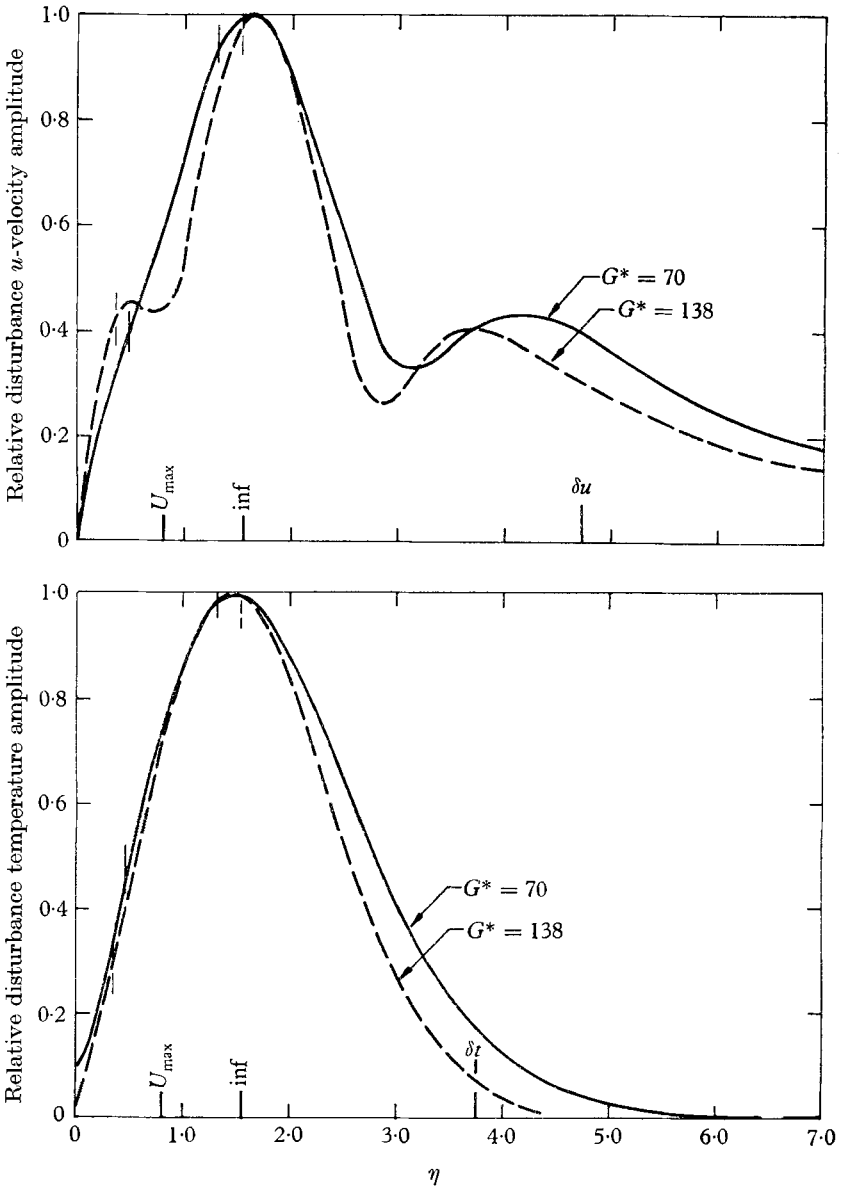

FIGURE 9. Theoretical disturbance amplitude distributions for Prandtl number = 0·733, uniform flux base flow and $Q^* = 0{\cdot}03$. Vertical lines indicate the locations of the critical layers. δu and δt indicate the outer edges of the velocity and thermal boundary layers.

haviour. Again, the relative phase change across the thermal boundary layer is approximately $\frac{1}{4}$-wave. The temperature phase distributions are discontinued beyond $\eta = 4$ for $Pr = 0{\cdot}733$ and $\eta = 3$ for $Pr = 6{\cdot}9$. For values of η greater than these the disturbance temperature distribution has gone to zero. The remaining temperature eigenfunctions consist of computer noise and hence a calculated phase angle is irrelevant.

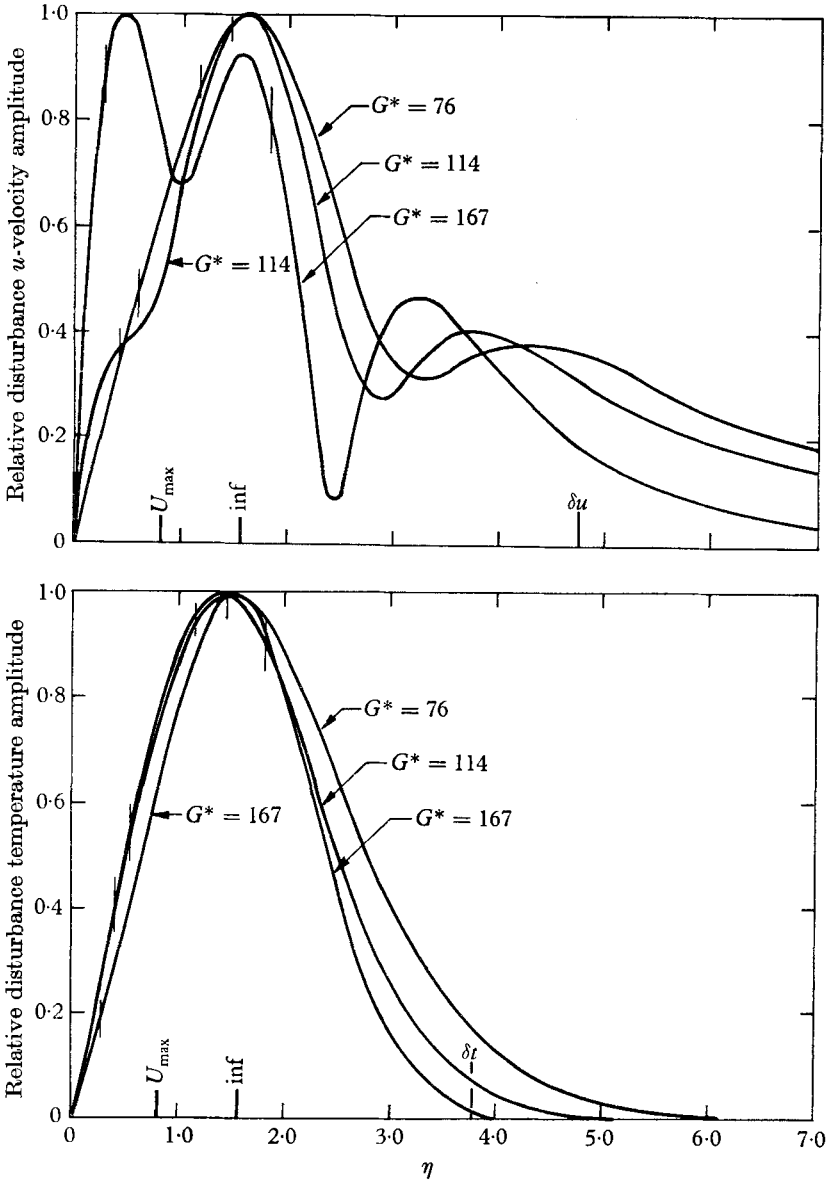

FIGURE 10. Theoretical disturbance amplitude distributions for Prandtl number = 0·733, uniform flux base flow and $s(0) = 0 (Q^* = \infty)$. Vertical lines indicate the locations of the critical layers. δu and δt indicate the outer edges of the velocity and thermal boundary layers.

The disturbance u-velocity phase distribution is also similar for both boundary conditions with $Pr = 0{\cdot}733$. These distributions show that the disturbance u-velocity undergoes a rather sudden phase change of more than $\frac{1}{2}$ wavelength

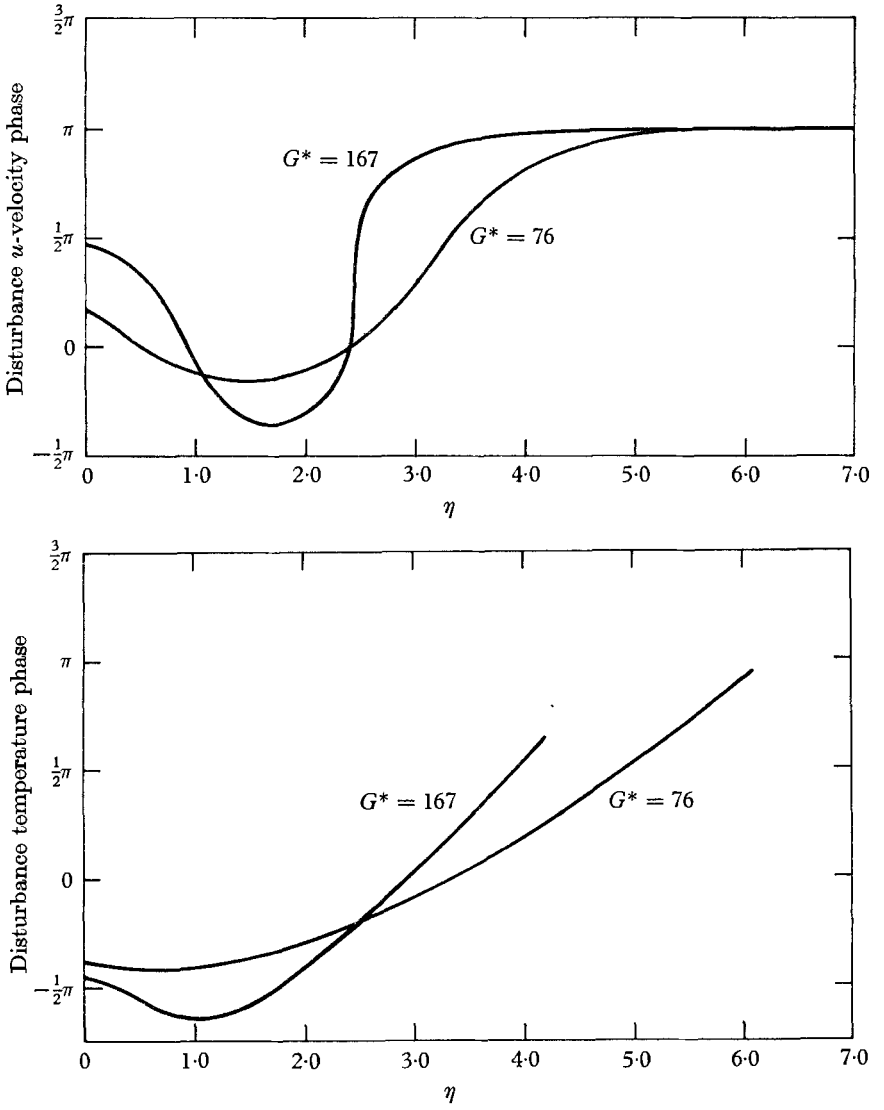

FIGURE 11. Disturbance u-velocity and temperature phase distributions for Prandtl number = 0·733, uniform flux base flow and $s(0) = 0$ ($Q^* = \infty$).

in the region of the outer edge of the thermal boundary layer. The distance in which this phase change occurs depends upon the magnitude of G^* for the thermal boundary condition that $s(0) = 0$. Between the range of G^* from 77 to 120 this is not the case for the boundary condition that $s'(0) = 0$. It would at first appear that this phase reversal is due to an uncoupling of the flow due to the fact that the base flow temperature distribution is reduced to approximately 5 % of its maximum. However, this same effect was predicted by Schlichting (1933),

and was observed experimentally by Schubauer & Skramstad (1948) for a forced flow in which no coupling is present. The location of this sudden phase change corresponds to the dip in the disturbance u-velocity distribution.

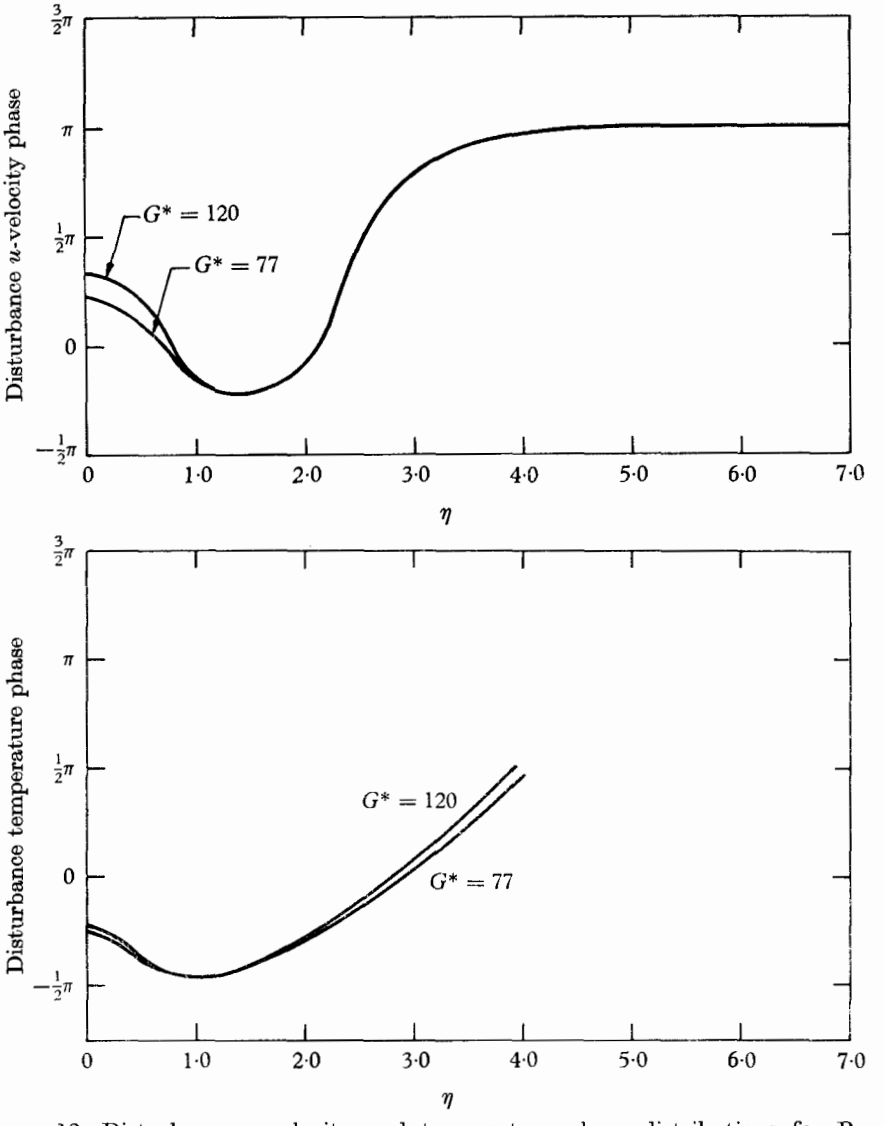

FIGURE 12. Disturbance u-velocity and temperature phase distributions for Prandtl number = 0·733, uniform flux base flow and $s'(0) = 0$.

5. Comparison of theory and existing experimental results

Figure 14 shows a comparison of the neutral stability curves for the coupled results of the present analysis for air (with $Pr = 0{\cdot}733$) with the uncoupled results† previously obtained by Polymeropoulos & Gebhart (1966), Nachtsheim

† The isothermal wall results of Nachtsheim (1963) and Kurtz & Crandall (1962) have been renormalized according to the technique of Polymeropoulos & Gebhart (1966).

(1963) and Kurtz & Crandall (1962). The effect of two different base flows on uncoupled solutions is relatively small. This is expected, due to the similarity of the temperature and velocity profiles for the two cases. However, the influence

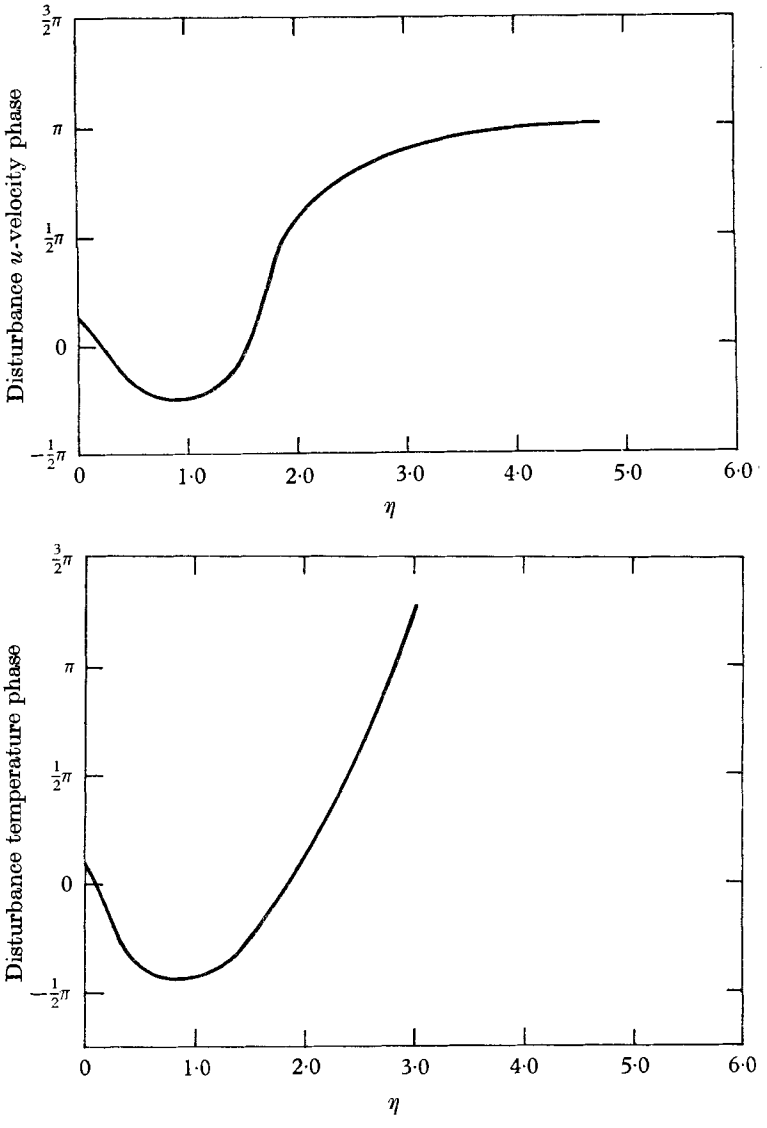

FIGURE 13. Disturbance u-velocity and temperature phase distributions for Prandtl number = 6·9, $G^* = 65$, uniform flux base flow and $s'(0) = 0$ ($Q^* = 0$).

of the temperature coupling in the disturbances depends strongly upon the disturbance-temperature boundary condition at the wall. It can be seen that, for the same disturbance-temperature boundary condition [$s(0) = 0$], the influence of the base flow upon the neutral stability curve is small for this Prandtl number. In both flow cases the temperature-coupling results in a distinctive departure from the uncoupled case for α less than 0·4. Above this value, the coupled curves

resemble the uncoupled curves. For large values of αG^* the coupled and uncoupled curves appear to become asymptotic.

However, the disturbance temperature boundary condition has a very pronounced effect on the neutral curve. For zero relative thermal capacity the temperature coupling appears to dominate the eigenvalue dependence upon G^* over the whole range. The curve does not even become asymptotic to the uncoupled curve (at least for $G^* \leqslant 173$).

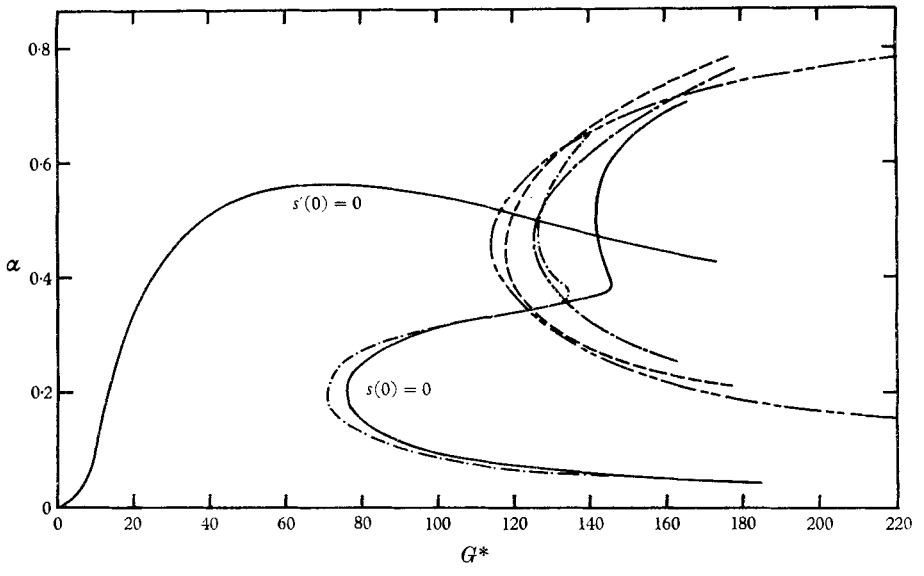

FIGURE 14. Comparison between neutral curves for isothermal wall and uniform flux base flows in air [the isothermal wall results have been re-normalized according to Polymeropoulos & Gebhart (1966)]. ——, present calculations, uniform flux, coupled; - - - -, Polymeropoulos & Gebhart (1966), uniform flux, uncoupled; —·—·, Nachtsheim (1963), isothermal wall, coupled; — — —, Nachtsheim (1963), isothermal wall, uncoupled; —— — —, Kurtz & Crandall (1962), isothermal wall, uncoupled.

The neutral curves calculated for higher Prandtl numbers (from 3 to 6·9) do not exhibit this limiting behaviour in the range of the solution. Figure 15 compares the uniform flux base flow results for Prandtl numbers of 5·0 and 6·9 and zero relative thermal capacity [$s'(0) = 0$] with the results of Nachtsheim (1963) for isothermal wall base flow [and $s(0) = 0$]. The uncoupled neutral curve of Nachtsheim is not within the scale of this figure; the nose of this curve is located at $G^* = 500$ and $\alpha = 0{\cdot}396$. (The isothermal-wall curve is re-normalized as discussed in the footnote on page 677 above). The effect of temperature-coupling is very pronounced in this Prandtl number range, resulting in a displacement of the nose of the isothermal-wall neutral curve by a factor of 10 in G^*.

The uniform-flux base flow results shown in figure 15 reflect not only the effect of the base flow, but also the effect of the new disturbance temperature boundary condition. While these changes result in an offset of the neutral curve, they do not cause a complete change in the shape of the curve as in the case of $Pr = 0{\cdot}733$.

The experimental results of Polymeropoulos & Gebhart (1967) are compared

with the present calculated results for air in figure 16. The data show clearly the effect of the disturbance temperature boundary condition. The experiment was conducted in pressurized nitrogen, with an electrically heated thin foil being used to generate the flow. Using both resistance thermometers and an interferometer, it was established that the foil temperature distribution corresponded to the theoretical results of Sparrow & Gregg (1956) for a uniform flux surface.

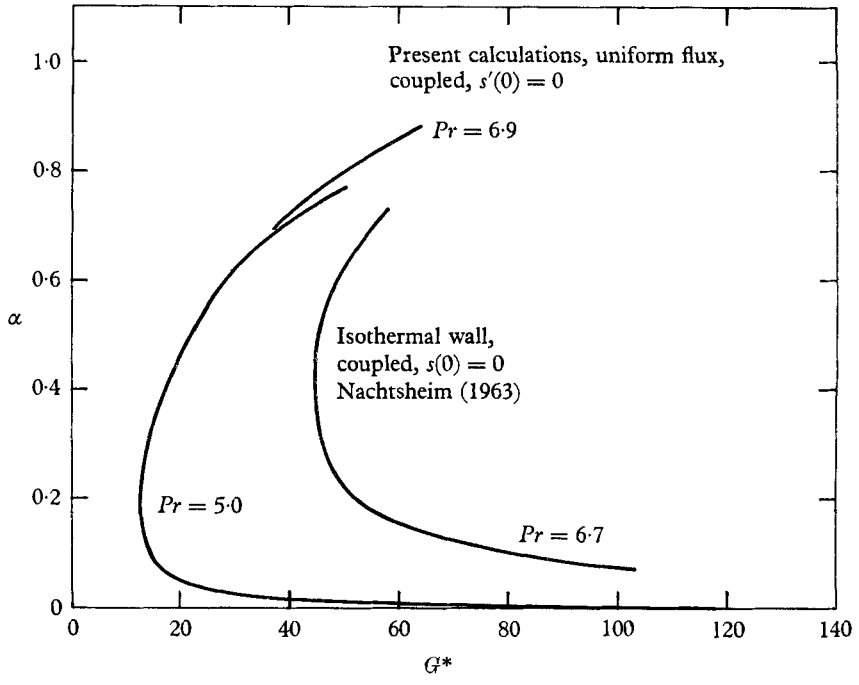

FIGURE 15. Comparison between neutral curves for isothermal wall and uniform flux base flows in higher Prandtl number fluids [the isothermal wall results have been renormalized according to Polymeropoulos & Gebhart (1966)].

Thus, it can be concluded for those experiments that the base flow was that of a uniform-flux surface condition. It is clear from figure 16, however, that the data is quite different from the solution for a boundary condition of zero disturbance flux at the plate.

Values of the storage parameter, Q^*, were computed for the data of Polymeropoulos & Gebhart (1967). It was found that for α less than 0·4, Q^* was greater than 0·04. As a result, these data are expected to (and do at low α) lie in the region bounded by the curves for $Q^* = 0{\cdot}03$ and $Q^* = \infty$.

It is apparent, therefore, that although the base flow was that of a uniform flux plate, the plate thermal capacity was sufficiently large compared to that of the pressurized nitrogen, that the wall almost, but not completely, damped out the disturbance temperature fluctuations.

The fringe amplitude distribution given in Polymeropoulos (1966) cannot be compared to the calculated disturbance temperature amplitude distributions directly, since the temperature change is proportional to the relative fringe shift.

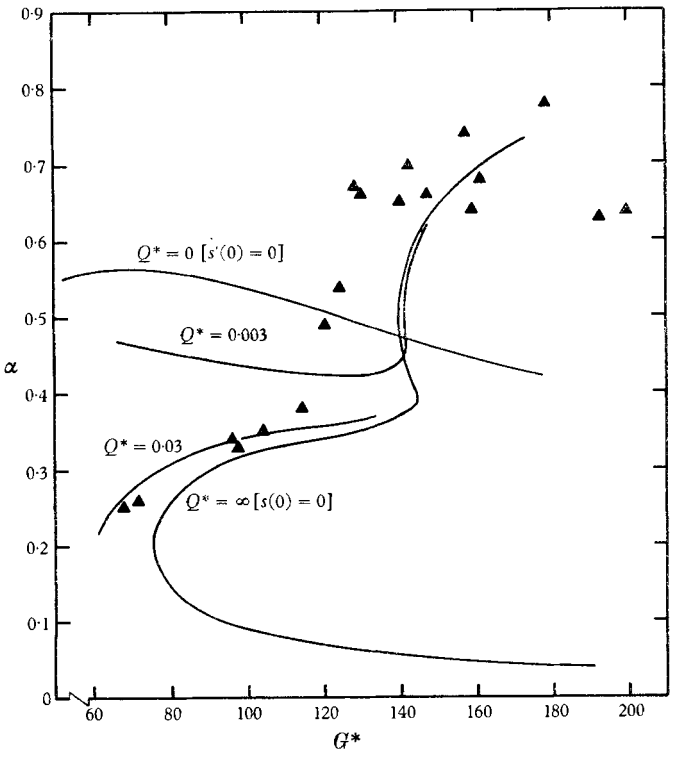

FIGURE 16. Comparison of experimental results of Polymeropoulos & Gebhart (1966) with theoretical neutral curves for air. ▲, experimental data, Polymeropoulos & Gebhart (1967).

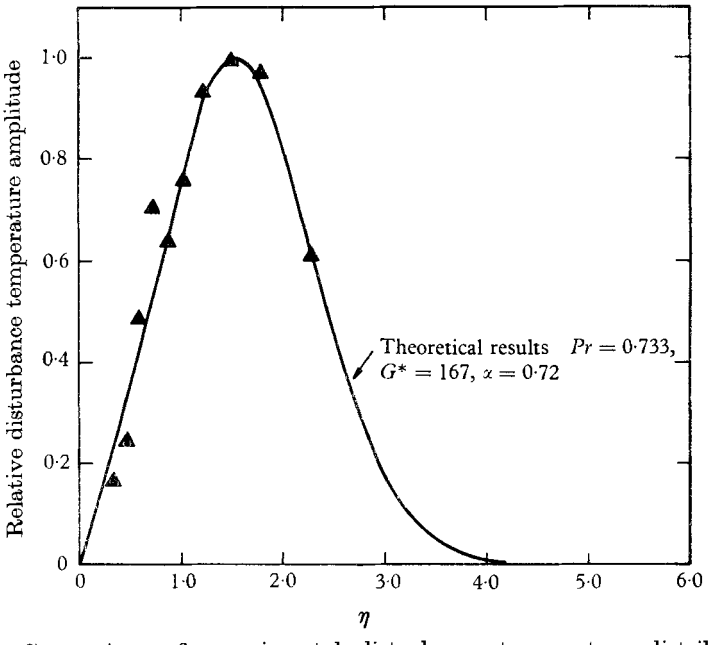

FIGURE 17. Comparison of experimental disturbance temperature distribution with theoretical distribution for air. ▲, experimental data. $Pr = 0{\cdot}72$, $G^* = 200$, $\alpha = 0{\cdot}64$, Polymeropoulos (1966, figure 40*a*).

Thus the fringe spacing must also be measured, and the fringe amplitude be divided by the average fringe spacing in order to obtain an experimental disturbance-temperature distribution.

One negative was available from the data of Polymeropoulos [figure 40*a* of Polymeropoulos (1966)] and it was remeasured. The results are shown in figure 17, along with the theoretical results for the $s(0) = 0$ boundary condition. The actual value of Q^* for these experimental data is 0·02. The theoretical solutions for $Q^* = 0{\cdot}03$ were not continued in the G^* range of these data, so that the comparison is made with the theory for $Q^* = \infty$. Figures 9 and 10 show, however, that the disturbance temperature amplitude distribution is very nearly the same for $Q^* = 0{\cdot}03$ and $Q^* = \infty$. The agreement between the data and the theory is remarkably good.

6. Conclusions

This study follows directly on other recent ones and collectively they greatly increase our understanding of conditions for laminar instability in external natural convection flows. Until recently very little was known about such stability because of the complexity of the theoretical equations and because of the ill-definition and rudimentary nature of the few previous experimental studies.

Following the first complete solution by Nachtsheim (1963) and the first critical experiments, reported by Polymeropoulos & Gebhart (1967), it was evident that a linear-disturbance theory, similar to that which has been so successful for boundary regions in forced flow, is equally applicable to the more complicated natural convection flows.

The present paper examines the questions of laminar instability in boundary region natural convection flow more closely. The weak nature of such flow processes, the inevitable coupling of velocity and temperature disturbances through buoyancy, the primacy of the fluid Prandtl number as a parameter, and the expected critical thermal capacity coupling between the surface and the flow disturbances pose questions which this paper considers, through the application of stability theory.

Since many natural convection flows result more nearly from a surface which uniformly generates heat than from an isothermal surface, the effect of different base flows on stability characteristics was determined. For the Prandtl number typical of gases, and non-zero values of wall relative thermal capacity, the effect is small. For larger Prandtl numbers, however, the effect is perhaps more important, probably through the changing relation between base-flow velocity and temperature boundary region thicknesses.

In many natural convection flows the thermal capacity of the element generating the flow is sufficiently small so that it couples in an important way with the thermal storage changes in the flow due to disturbances. Allowing for this effect amounts to modifying the boundary conditions for the stability equations. A thermal capacity parameter arises which is similar to that already shown to be crucial in describing transients in natural convection flows. The use

		Fluid properties				Foil properties			
Fluid	Foil material	Pr	ρ (lb./ft.^{3})	x_n (in.)	C_p B.Th.U./lb. °F	ρ (lb./ft.^{3})	Thickness (in.)	C (B.Th.U./lb. °F)	Q^*
Air at Std Cond.	Inconel	0·72	0·074	12	0·24	530·5	0·0026	0·109	0·10
	Inconel	0·72	0·074	12	0·24	530·5	0·00026	0·109	0·01
Air at 20 atmos.	Inconel	0·72	1·48	12	0·24	530·5	0·0051	0·109	0·01
	Inconel	0·72	1·48	12	0·24	530·5	0·0005	0·109	0·001
Water at 70 °F	Inconel	6·32	62·3	12	0·998	530·5	0·0938	0·109	0·01
	Inconel	6·32	62·3	12	0·998	530·5	0·0094	0·109	0·001
Mercury at 70 °F	Inconel	0·0288	850·78	12	0·0335	530·5	1·027	0·109	0·001

Table of typical Q^* values for various fluids and foil thicknesses

of this more realistic type of boundary condition, for practical configurations, results in variability in the conditions for incipient laminar instability. The effects are very large. Through the use of such information, the temperature coupling evidence of previous experimentation is more completely explained.

Much information is presented concerning distributions of disturbance quantities across the boundary regions and their changes with Prandtl number and relative thermal capacity. The locations of disturbance maxima and distributions of phase angle are very interesting, especially when compared with the classical ideas, such as the critical layer, which were prevalent in the earlier approximate solutions of the stability equations. An experimentally determined disturbance temperature distribution is compared with one calculated from stability theory, with good agreement.

All stability analysis to date in natural convection flows has been carried in terms of two-dimensional disturbances. In the appendix it is shown that, for temperature and velocity disturbances coupling through buoyancy, the flow is unstable at lower Grashof number for two-dimensional than for three-dimensional disturbances.

The authors wish to express appreciation for National Science Foundation support in this research, and in preparation of the paper, under research grants GP-127 and GK-1963. They would also like to thank Dr R. P. Dring and Mr C. A. Hieber for help and advice in computations and in paper preparation.

Appendix. Extension of Squires theorem to coupled disturbances in natural convection

It has been shown by Squire (1933) for forced flow that two-dimensional disturbances will develop at a lower Reynolds number than three-dimensional disturbances. It will be shown that this result can be extended to the case of temperature-coupled natural convection disturbances.

For this purpose, consider the natural convection flow over a vertical flat plate of infinite span with the co-ordinate system as shown in figure 1. The governing linearized perturbation equations, assuming one-dimensional base flow, can be reduced to

$$\frac{\partial u}{\partial x}+\frac{\partial y}{\partial v}+\frac{\partial w}{\partial z}=0, \tag{A 1}$$

$$\frac{\partial \Omega_x}{\partial \bar{\tau}}+U\frac{\partial \Omega_x}{\partial x}+\frac{dU}{dy}\frac{\partial w}{\partial x}=\nu\nabla^2\Omega_x, \tag{A 2}$$

$$\frac{\partial \Omega_y}{\partial \bar{\tau}}+U\frac{\partial \Omega_y}{\partial x}+\frac{dU}{dy}\frac{\partial v}{\partial z}=\nu\nabla^2\Omega_y+g\hat{\beta}\frac{\partial t}{\partial z}, \tag{A 3}$$

$$\frac{\partial \Omega_z}{\partial \bar{\tau}}+U\frac{\partial \Omega_z}{\partial x}-v\frac{d^2U}{dy^2}+\frac{dU}{dy}\frac{\partial w}{\partial z}=\nu\nabla^2\Omega_z-g\beta\frac{\partial t}{\partial y} \tag{A 4}$$

and

$$\frac{\partial t}{\partial \bar{\tau}}+U\frac{\partial t}{\partial x}+v\frac{dT}{dy}=\frac{k}{\rho\hat{c}}\nabla^2 t, \tag{A 5}$$

where $$\Omega_x = \frac{\partial w}{\partial y} - \frac{\partial v}{\partial z}; \quad \Omega_y = \frac{\partial u}{\partial z} - \frac{\partial w}{\partial x}; \quad \Omega_z = \frac{\partial v}{\partial x} - \frac{\partial u}{\partial y}.$$

The disturbance quantities are assumed to be periodic in x, z and $\bar{\tau}$ so that

$$u(x, y, z, \bar{\tau}) = \bar{u}(y) \exp i(\bar{a}x + \bar{b}z - \bar{a}\bar{c}\bar{\tau}), \quad \text{etc.}$$

Substituting these quantities in the governing equations and normalizing as before, the following equations for v and t are obtained†

$$(F' - c)\left[\frac{d^2v}{d\eta^2} - (a^2 + b^2)v\right] + \frac{i}{a\hat{G}^*}\left[\frac{d^4v}{d\eta^4} - 2(a^2 + b^2)\frac{d^2v}{d\eta^2} + (a^2 + b^2)^2 v\right] - F'''v + \frac{1}{\hat{G}^* Pr}\frac{dt}{d\eta} = 0 \quad \text{(A 6)}$$

and $$H'v + iaF' - ct = \frac{1}{\hat{G}^* Pr}\left[\frac{d^2t}{d\eta^2} - (a^2 + b^2)t\right]. \quad \text{(A 7)}$$

With the further substitutions

$$v = -ia\Phi \quad \text{and} \quad t = s,$$

(A 6) and (A 7) can be written as

$$(F' - c)[\Phi'' - (a^2 + b^2)\Phi] - F'''\Phi = -\frac{i}{a\hat{G}^*}[\Phi^{iv} - 2(a^2 + b^2)\Phi'' + (a^2 + b^2)^2\Phi + s'] \quad \text{(A 8)}$$

and $$(F' - c)s - H'\Phi = -\frac{i}{a\hat{G}^* Pr}[s'' - (a^2 + b^2)s]. \quad \text{(A 9)}$$

These two equations are identical to the corresponding two-dimensional equations if

$$\alpha^2 = a^2 + b^2$$

and $$\alpha G^* = a\hat{G}^*.$$

Since a, b and α are all real for a neutral disturbance, the first equation requires that $\alpha > a$ and hence the second equation shows that $G^* < \hat{G}^*$, i.e. that the two-dimensional critical Grashof parameter is smaller than the corresponding three-dimensional Grashof parameter. As a result, for an infinite span, the flow will be most unstable for the two-dimensional disturbances.

This fact has been observed experimentally in pressurized nitrogen by Polymeropoulos (1966) and in 0·65 ctsk. silicone by the first author, Knowles (1967), for foil aspect ratios of approximately 6:1.

REFERENCES

Birch, W. D. 1957 M. S. Thesis, Air University, Wright–Patterson Air Force Base.

Colak-Antic, P. 1964 *Jahrbuch der WGLR*, 171.

Dunn, D. W. & Lin, C. C. 1955 *J. Aeronaut. Sci.* **22**, 455.

Eckert, E. R. G. & Soehngen, E. 1951 *Proc. Gen. Disc. Ht. Tr. Lond.* 321.

Gartrell, H. E. 1959 M.S. Thesis, Air University, Wright-Patterson Air Force Base.

Gebhart, B. 1963 *J. Heat Trans.* **85**, 10.

† In order to avoid excessive nomenclature, the same symbol will be used for the dimensional and normalized quantities v and t.

KNOWLES, C. P. 1967 Ph.D. Thesis, Cornell University.
KURTZ, E. F. & CRANDALL, S. H. 1962 *J. Math. Phys.* **41**, 264.
NACHTSHEIM, P. R. 1963 *Nat. Aero. Space Adm. TN* D-2089.
PLAPP, J. E. 1957 Ph.D. Thesis, Cal. Inst. of Tech.
POLYMEROPOULOS, C. E. 1966 Ph.D. Thesis, Cornell University.
POLYMEROPOULOS, C. E. & GEBHART, B. 1966 *AIAA J.* **4**, 2066.
POLYMEROPOULOS, C. E. & GEBHART, B. 1967 *J. Fluid Mech.* **30**, 225.
SCHLICHTING, H. 1933 *Nachr. Ges. Wiss. Gott. Math.-phys. Kl.* 181.
SHEN, S. F. 1954 *J. Aeronaut. Sci.* **21**, 62.
SCHUBAUER, G. B. & SKRAMSTAD, H. K. 1948 *Nat. Adv. Com. Aero. Rept.* 909.
SPARROW, E. M. & GREGG, J. L. 1956 *ASME Trans.* **78**, 435.
SPARROW, E. M., TSOU, F. K. & KURTZ, E. F. 1965 *Phys. Fluids*, **8**, 1559.
SQUIRE, H. B. 1933 *Proc. Roy. Soc.* A **142**, 621.
SZEWCZYK, A. A. 1962 *Int. J. Ht. Mass. Tr.* **5**, 903.
TOLLMIEN, W. 1931 *Nat. Adv. Com. Aero. TM* 609.